Structural Basis for Stereoselectivity in the (*R*)- and (*S*)-Hydroxypropylthioethanesulfonate Dehydrogenases[†,‡]

Arathi M. Krishnakumar,[§] Boguslaw P. Nocek,[§] Daniel D. Clark,[||] Scott A. Ensign,[||] and John W. Peters*[,§]

Department of Chemistry and Biochemistry, Montana State University, Bozeman, Montana 59717, and Department of Chemistry and Biochemistry, Utah State University, Logan, Utah 84322

Received February 20, 2006; Revised Manuscript Received May 22, 2006

ABSTRACT: Epoxide metabolism in *Xanthobacter autotrophicus* Py2 results in the conversion of epoxypropane to acetoacetate. Epoxide metabolism is initiated by the nucleophilic addition of coenzyme M to the (*R*)- and (*S*)-enantiomers of epoxypropane which forms the respective enantiomers of 2-hydroxypropyl-coenyme M. The (*R*)- and (*S*)-enantiomers of 2-hydroxypropyl coenzyme are oxidized to the achiral product 2-ketopropyl-CoM by two stereoselective dehydrogenases. The dehydrogenases catalyzing these reactions, termed (*R*)-hydroxypropyl-coenzyme M dehydrogenase (*R*-HPCDH) and (*S*)-hydroxypropyl-coenzyme M dehydrogenase (*S*-HPCDH), are NAD$^+$-dependent enzymes belonging to the short chain dehydrogenase/reductase (SDR) family of enzymes. In this study, the crystal structure of *R*-HPCDH cocrystallized in the presence of (*S*)-hydroxypropyl-coenzyme M has been determined using X-ray diffraction methods and refined to 1.8 Å resolution. The structure of *R*-HPCDH is tetrameric and stabilized by the interaction of the terminal carboxylates of each subunit with divalent metal ions. The structure of the presumed product-bound state reveals that binding interactions between the negatively charged oxygen atoms of the sulfonate moiety have striking similarities to sulfonate interactions observed in the previously determined structure of 2-ketopropyl-CoM oxidoreductase/carboxylase, highlighting the utility of coenzyme M as a carrier molecule in the pathway. The key elements of the aforementioned interactions are electrostatic interactions between the sulfonate oxygen atoms and two arginine residues (R152 and R196) of *R*-HPCDH. The comparison of the structure of *R*-HPCDH with a homology model of *S*-HPCDH provides a structural basis for a mechanism of substrate specificity in which the binding of the substrate sulfonate moiety at distinct sites on each stereoselective enzyme directs the orientation of the appropriate substrate enantiomer for hydride abstraction.

The highly reactive nature of epoxides makes them valuable intermediates for the synthesis of more complex optically active or biologically active compounds, including pharmaceuticals and agrichemicals. For this reason, there has been considerable interest in exploiting epoxide-utilizing enzymes which have stereoselective and regioselective properties for producing enantiopure compounds. Some of the known alkene-oxidizing enzymes, such as heme-dependent monooxygenases, ω-hydroxylases, and non-heme oxygenases, catalyze direct stereospecific epoxidation of alkenes (*1*). Alternatively, enantiopure epoxides can be resolved from racemic mixtures by enantioselective epoxide metabolizing enzymes. Some microorganisms are capable of utilizing aliphatic alkenes and epoxides as sole carbon sources (*2*). The pathway for the metabolism of short chain alkenes and epoxides in aerobic bacterium *Xanthobacter autotrophicus* Py2 has been well-characterized (*3*−*8*). Integral to this metabolic pathway are the two stereospecific 2-hydroxypropylthioethanesulfonate dehydrogenases designated *R*-HPCDH[1] and *S*-HPCDH that individually allow for the oxidation of only (*R*)- and (*S*)-epoxypropane enantiomers, respectively, to the common achiral product 2-ketopropylthioethanesulfonate or 2-ketopropyl-CoM.

The two dehydrogenases, *R*-HPCDH and *S*-HPCDH, are related with 41% similar sequences and belong to the short chain dehydrogenase reductase superfamily of enzymes (*8*). Enzymes of this class are approximately 250 amino acids in

[1] Abbreviations: *R*-HPC, 2-(*R*)-hydroxypropylthioethanesulfonate; *S*-HPC, 2-(*S*)-hydroxypropylthioethanesulfonate; *R*-HPCDH, 2-(*R*)-hydroxypropylthioethanesulfonate dehydrogenase; *S*-HPCDH, 2-(*S*)-hydroxypropylthioethanesulfonate dehydrogenase; SDR, short chain dehydrogenase reductase; 2-KPC, 2 ketopropylthioethanesulfonate; CoM, coenzyme M (2-mercaptoethanesulfonate); 2-KPCC, 2-ketopropyl-CoM oxidoreductase/carboxylase; MAD, multiple-wavelength anomalous diffraction; NAD$^+$ and NADH, nicotinamide adenine dinucleotide; NADP$^+$, nicotinamide adenine dinucleotide phosphate; MDH, mannitol dehydrogenase; HADH, halo alcohol dehydrogenase.
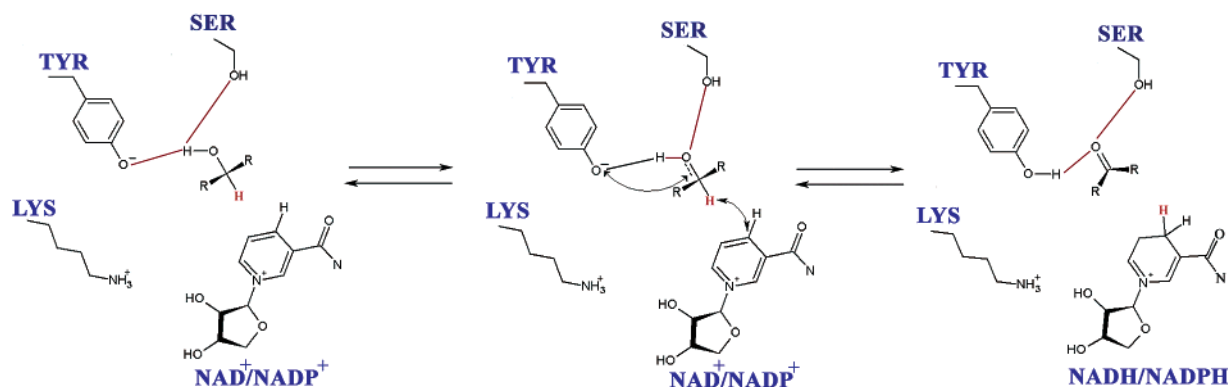
FIGURE 1: General mechanism of SDR enzymes involving the conserved serine, tyrosine, and lysine catalytic triad.
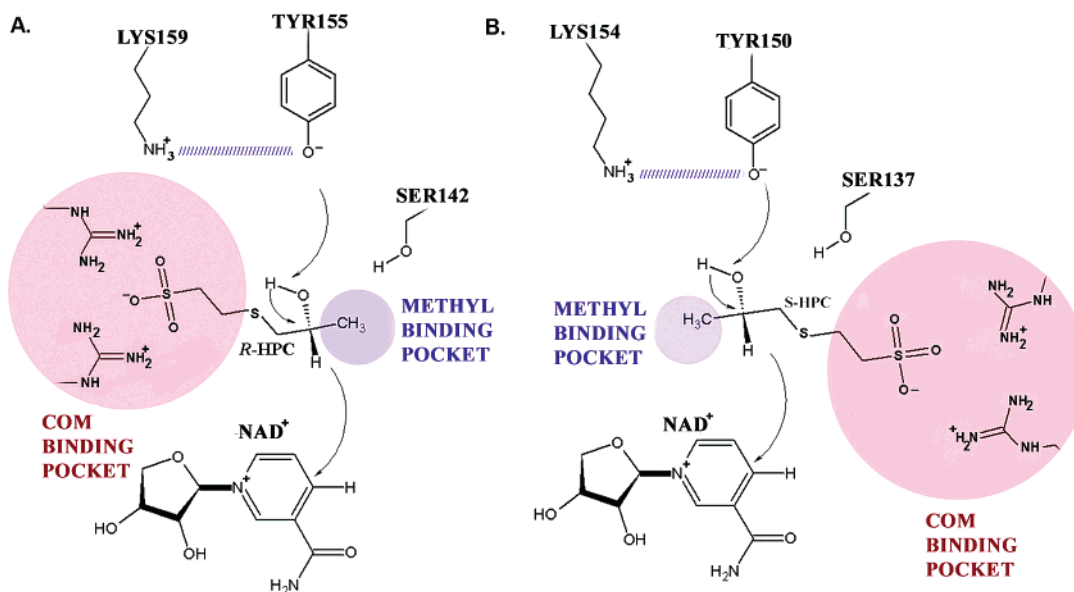

FIGURE 2: Models for binding of the substrate to (A) *R*-HPCDH and (B) *S*-HPCDH for stereospecific dehydrogenation of the enantiomers of 2-hydroxypropyl-CoM.

length and exist as dimers or tetramers in solution (*9*). The culmination of structural, kinetic, and mechanistic studies on the SDR enzymes has resulted in the formulation of a general mechanism of action presented in Figure 1 (*10*). On the basis of this and sequence alignments along with site-directed mutagenesis studies, the identity and function of the catalytic residues have been established for *R*-HPCDH (*11*). Residues Tyr155, Lys159, and Ser142 form the catalytic triad, and their functions are consistent with the general mechanism (Figure 1). According to this, the tyrosyl hydroxyl is deprotonated which then serves as a general base for proton abstraction from the hydroxyl group of the substrate. The amino group of lysine stabilizes the deprotonated Tyr general base. Serine is thought to increase the acidity of the substrate hydroxyl through hydrogen bonding.

Although the dehydrogenases are in most cases stereospecific, there is only one other case known in which pairs of stereospecific dehydrogenases act in concert in one pathway. Tropinone reductase I and II from *Datura stramonium* (TR-I and TR-II, respectively) catalyze the reversible stereospecific reduction of the 3-keto group of tropinone to form the enantiomers tropine (α-hydroxy) and pseudotropine (β-hydroxy), respectively (*12*, *13*). Structural characterization of TR-I and TR-II has revealed that electrostatic interactions between substrates and charged amino acids in the active

site were responsible for orienting the substrate to its correct geometry. For TR-I, a positively charged histidine nitrogen (His112) repels the positive charge on the nitrogen atom of tropinone and serves to orient the substrate in the active site. In the case of TR-II, the negatively charged glutamate carboxylate (Glu156) attracts the substrate nitrogen and thus fixes its position.

Our recent work involving amino acid modification in *R*-HPCDH has implicated the involvement of two arginine residues (Arg196 and Arg152) in substrate binding (*14*). These residues have been proposed to support substrate binding through electrostatic interactions between the positively charged arginine side chains and the negatively charged oxygen atoms of the substrate sulfonate group. In the context of this proposal, our structural studies have revealed that the binding of substrate for 2-KPCC, which catalyzes the next step in the pathway, is mediated by interactions between two arginine residues (Arg56 and Arg365) and the substrate sulfonate oxygens (*15*). The negatively charged sulfonate group offers a convenient "handle" on the substrate molecule for binding to the active site. Presumably, similar interactions between the sulfonate binding group and positively charged amino acid side chains are involved in the binding of substrate in both *R*- and *S*-HPCDH. On the basis of the aforementioned site-directed mutagenesis studies of *R*-

HPCDH and the crystal structure of 2-KPCC, a model has been proposed for the basis of stereoselectivity in which distinct sulfonate binding sites in *R*- and *S*-HPCDH promote the correct orientation for hydride abstraction of their respective substrates (Figure 2).

For the tropinone reductases, the three-dimensional structures were the key to defining the mechanism and structural basis of stereoselectivity. In the study presented here, the three-dimensional structure of *R*-HPCDH reveals the features of the substrate binding site that contribute to stereoselective hydride abstraction. A combination of substrate docking and homology modeling studies together with the structural analysis of *R*-HPCDH indicates that the difference in binding of the negatively charged sulfonate group of the substrate in the C-terminal substrate binding domain of each enzyme is the key to chiral discrimination.

EXPERIMENTAL PROCEDURES

Crystals of 2-*R*-HPCDH can be obtained in three crystal forms, two of which exist with $P2_1$ space group symmetry and one with $C2$ (*16*). The $C2$ crystal form grown in the absence of substrates or inhibitors is of poor to moderate diffraction quality such that data to ~3 Å resolution can be collected routinely at a synchrotron source. A $P2_1$ crystal form of similar quality can also be grown in the absence of substrates or inhibitors. An additional $P2_1$ crystal form with significantly better diffraction (better than 2.0 Å resolution) is obtained when crystals are grown in the presence of substrates or inhibitors and NAD$^+$ (*16*). Although the primary sequence is considerably identical with the sequences of members of the SDR family, attempts to determine the structure by molecular replacement methods in any of the aforementioned crystal forms were unsuccessful. A significant impediment to determining the structure by molecular replacement was most likely that each crystal exists with multiple (four to eight) SDR subunits per asymmetric unit.

Since molecular replacement did not yield a reliable solution, the structure was determined by the multiple-wavelength anomalous diffraction (MAD) methods. MAD studies were conducted using a mercury heavy atom derivative of the enzyme. To generate the *R*-HPCDH mercury derivative, native $P2_1$ crystals were grown in the presence of 2 mM ethylmercury thiosalicylic acid (EMTS) with 0.17 M ammonium acetate, 0.085 M tri-sodium citrate dehydrate pH 5.6, 25.5% w/v polyethylene glycol 4000, and 15% v/v glycerol anhydrous (*17*). A three-wavelength MAD data set was collected at SSRL beam line 9-2 equipped with a mar345 imaging plate detector (Mar USA, Inc.). Data were processed with DENZO (*18*) and scaled with SCALPACK (*18*) of the HKL or HKL2000 program suite, and the data collection statistics are summarized in Table 1. The positions of heavy atom binding sites in the MAD experiment were identified using SOLVE (*19*). Initial searches and refinement of nine heavy atom sites per unit cell resulted in a figure of merit of 0.46 from 20.0 to 3.2 Å resolution. The heavy atom sites were utilized in RESOLVE (*19*) to identify noncrystallographic 2-fold operation and resulted in an improvement in the figure of merit of 0.60. The automated model building routine of RESOLVE could produce a partial model of the structure, and the remaining regions of the molecule were built manually into the initial phase-extended maps using the model building program O (*20*). The structure refinement

Table 1: Multiple-Wavelength Anomalous Diffraction Data Statistics

cell dimensions	$a = 67.149$ Å		
	$b = 124.178$ Å		
	$c = 121.908$ Å		
	$\beta = 100.742°$		

	peak ($\lambda = 0.87008$ Å)	remote ($\lambda = 1.00871$ Å)	inflection ($\lambda = 0.87278$ Å)
resolution (Å)	50.0−3.00	50.0−3.00	50.0−3.00
completeness (%)	99.9 (99.9)^a	99.9 (99.9)^a	99.9 (99.9)^a
no. of observed reflections	772150	921887	1440602
no. of unique reflections	290461	276477	264,138
I/σ	8.5 (8.4)^a	9.7 (9.1)^a	10.1 (6.5)^a
$R_{merge}{}^b$	0.066 (0.167)^a	0.072 (0.176)^a	0.077 (0.184)^a

^{a} Numbers in parentheses are values for the highest-resolution bin.
^{b} $R_{merge} = \sum_{hkl}\sum_i|I_i - \langle I\rangle|/\sum_{hkl}\sum_i|\langle I\rangle|$, where I_i is the intensity for the *i*th measurement of an equivalent reflection with indices *h*, *k*, and *l*.

Table 2: Data Statistics for *R*-HPCDH Cocrystallized with *S*-HPC

space group	$P2_1$
cell dimensions	$a = 64.44$ Å
	$b = 110.28$ Å
	$c = 68.98$ Å
	$\beta = 93.88°$
resolution (Å)	20.00−1.8
completeness (%)	93.9 (95.2)^a
no. of observed reflections	149113
no. of unique reflections	71201
I/σ	6.5 (2.1)^a
$R_{merge}{}^b$	0.084 (0.303)^a

^{a} Numbers in parentheses are values for the highest-resolution bin.
^{b} $R_{merge} = \sum_{hkl}\sum_i|I_i - \langle I\rangle|/\sum_{hkl}\sum_i|\langle I\rangle|$, where I_i is the intensity for the *i*th measurement of an equivalent reflection with indices *h*, *k*, and *l*.

Table 3: Refinement Statistics

resolution (Å)	20.00−1.80
R_{free}	0.197
R_{cryst}	0.227
no. of non-hydrogen atoms	
protein	4004
cofactor	176
product	44
solvent	915
rmsd from target values	
bond lengths (Å)	0.012
bond angles (deg)	1.55
average isotropic B factor	
all atoms	21.83
protein main chain	16.94
protein side chain	21.58
NAD$^+$	55.98
KPC	74.22
water	35.08

was carried out using CNS (*21*) from 50 to 3.0 Å with a 0σ cutoff with 5% of the data set aside for the calculation of R_{free} (*22*). The structure was subjected to multiple rounds of refinement and model building to generate a model suitable for a molecular replacement search model for the other crystal forms.

When the R_{free} of the native $P2_1$ crystal structure dropped just below 30%, this structure was used as a search model for molecular replacement to determine the structure of the substrate- and inhibitor-bound enzyme. Using CNS, a solution with four subunits in the asymmetric unit resulted in a correlation coefficient of 0.659 and an *R* factor of 0.381 with very good protein packing interactions. A well-determined
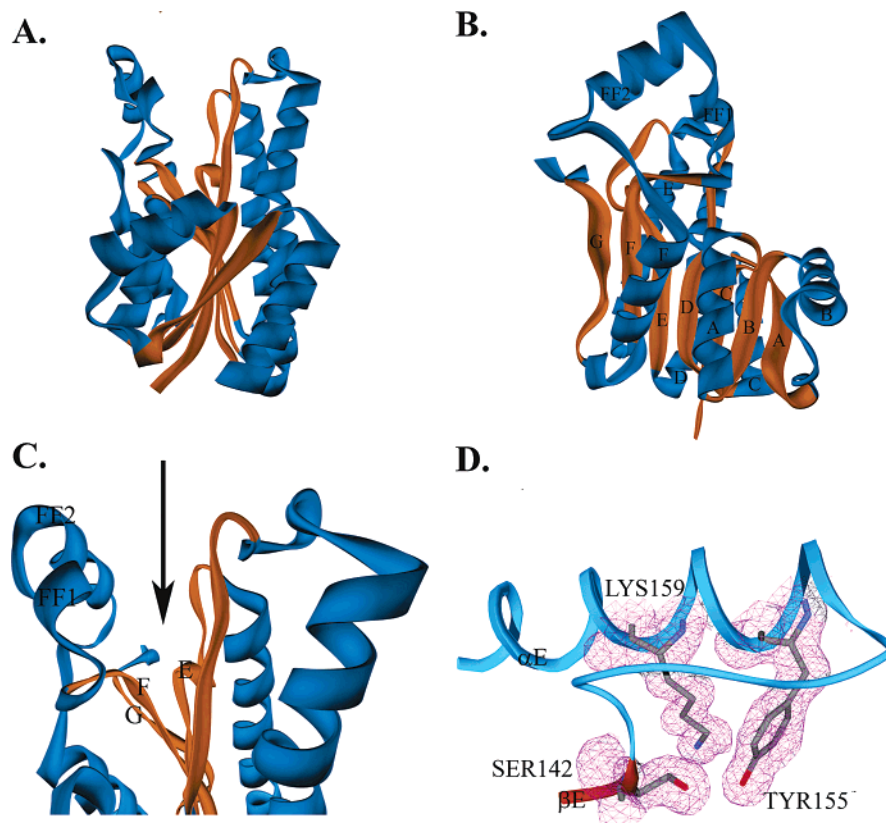
A.

B.

C.

D.

FIGURE 3: (A) Overall tertiary structure of one of the subunits of *R*-HPCDH with β strands colored orange and α-helices colored cyan displaying the twisted β sheet or the typical Rossmann fold. Bound NAD$^+$ is shown in Corey−Pauling−Koltun (CPK) representation. (B) Alternate view of the same subunit. (C) Zoomed-in view of the same subunit with an arrow pointing toward the substrate binding cleft. (D) Electron density maps ($2F_o - F_c$) contoured at 1σ about the residues forming the catalytic triad of *R*-HPCDH.

structure was obtained through multiple rounds of model building using O followed by refinement using CNS for data from 20 to 1.8 Å with a 0σ cutoff. The data statistics and refinement statistics of the native and the substrate−product cocrystal structure are summarized in Tables 2 and 3, respectively. The final models obey reasonable stereochemistry with 100% of the residues occupying allowed regions of a Ramachandran plot calculated using PROCHECK (*23*). The final structure of *R*-HPCDH and similar structures such as mannitol dehydrogenase and levodione reductase (*24*) were then used as templates to generate a homology model of *S*-HPCDH using the CPHMODEL (*25*) and SWISS MODEL (*26*) servers. All figures were generated using SWISS PDB VIEWER (*27*) and rendered using POVRAY (http://www.povray.org/povlegal.html).

RESULTS AND DISCUSSION

Overall Structure. The tertiary structure of each *R*-HPCDH subunit is a classic Rossmann fold common for the SDR family of enzymes. An overall α/β type structure has an open twisted parallel seven-stranded β sheet in the middle surrounded by six α helices (Figure 3A). Each subunit consists of two βαβαβ motifs, βA-αB-βB-αC-βC and βD-αE-βE-αF-βF, exhibiting right-handed crossover (*28*) by a seventh β strand with a left-handed crossover connection between β strands F and G (Figure 3B). The active site lies in the central region of each subunit, and catalytic residues Ser142, Tyr155, and Lys159 are located on βE and αE. The active site is located in a deep cleft which is lined on one side by two short helices, αFF1 (residues 192−201) and αFF2 (residues

202−211) (Figure 3C). The analogous region in other SDR enzymes has been shown to be responsible for substrate specificity (*29*). The other side of the active site cavity is lined by the loop formed between βE and βF (residues 143−153). The residues of the active site are very well resolved, and the electron density map in the region is excellent, allowing unambiguous assignment of positions of all the atoms in the side chains (Figure 3D). The position of the active site residues is consistent with their function in the proposed general mechanism of the SDR enzymes (Figure 1). Tyrosine acts as a general base for proton abstraction from the alcohol substrate, while lysine 159 is important in cofactor binding and in lowering the pK_a of the hydroxyl group of the tyrosine. Serine 142 coordinates the substrate hydroxyl group.

The quaternary structure of *R*-HPCDH (Figure 4A) is very similar to the tetrameric structures observed for other members of the SDR family, including mannitol dehydrogenase (MDH) (*30*) (Figure 4B) and halo alcohol dehydrogenase (HADH) (*31*). Previously, size exclusion chromatography suggested that *R*-HPCDH exists as a dimer in solution (*8*); however, the crystal structure suggests that the enzyme exists as a tetramer. The three-dimensional structure of *R*-HPCDH indicates four subunits related by 222 symmetry with dimensions of 71 Å × 61 Å × 59 Å. Interactions between individual monomers are along three noncrystallographic 2-fold axes analogous to that of the previously characterized SDR tetramers (*30*, *31*). The degree of interaction between the subunits of the putative tetramer is far too extensive for typical crystal packing interactions and involves a number of hydrophobic interactions. The specific interac-
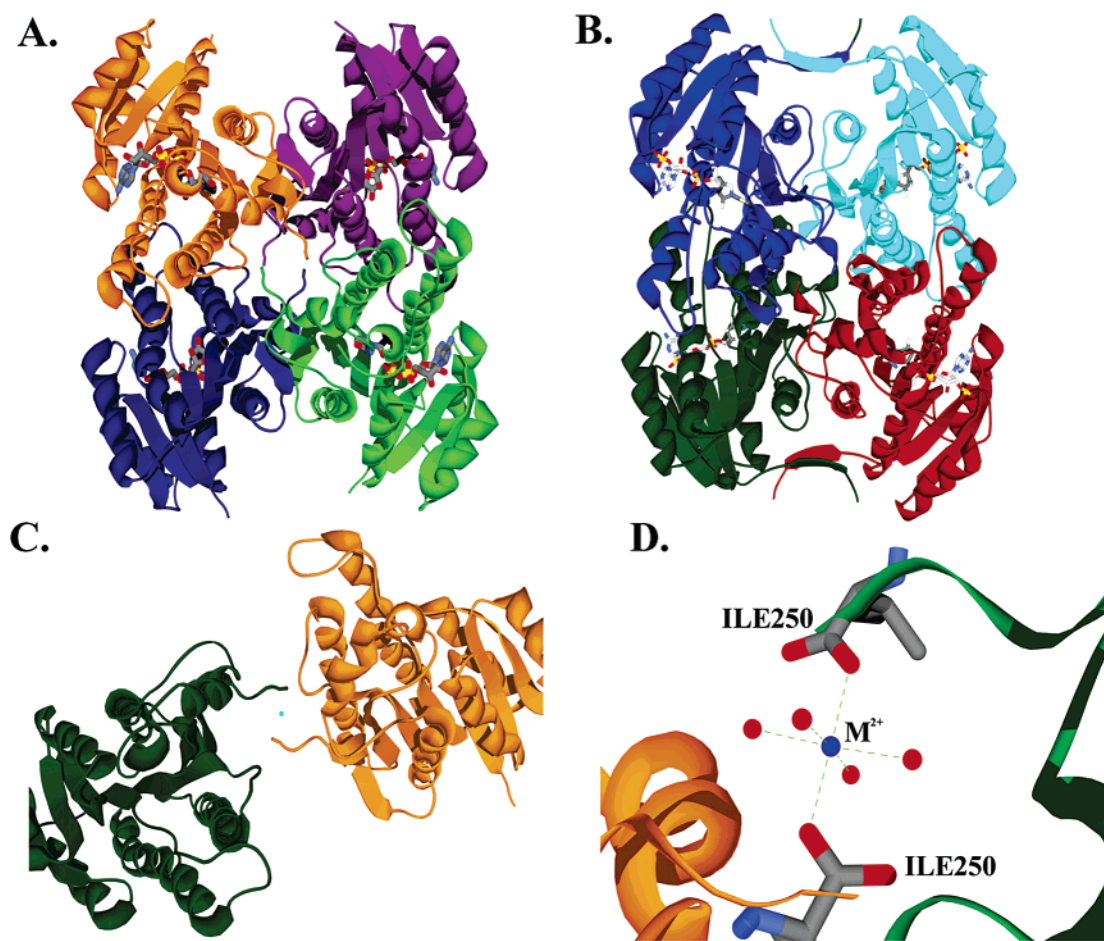
FIGURE 4: (A) Overall fold of tetrameric *R*-HPCDH with individual subunits colored blue, green, orange, and magenta. (B) Overall fold of the well-characterized mannitol dehydrogenase in the same orientation as the structure of *R*-HPCDH shown in panel A with the individual subunits colored blue, cyan, green, and dark red. (C) Two subunits of *R*-HPCDH held together at the C-terminus by a divalent metal colored blue via the terminal isoleucine residues. (D) Zoomed-in view of the divalent metal site coordinated by carboxylates of isoleucines supplied by two subunits of the enzyme and four water molecules at the equatorial position.

tions that stabilize the tetramers are very similar in MDH, HADH, and *R*-HPCDH. Interestingly, the tetrameric structure appears to be stabilized by the interaction of the C-termini with what are presumed to be divalent metal ions (Figure 4C). The metal ions are coordinated in a monodentate fashion at the axial position by one of the oxygens of the C-terminal carboxylate group of Ile250 supplied by each monomer and by four water molecules at the equatorial positions (Figure 4D). An analogous metal coordination is observed in the structure of mannitol dehydrogenase where the C-terminal tryptophans were observed to be coordinated by nickel ions (*30*). The identity of the metal ion in *R*-HPCDH has not been determined.

Interactions of NAD+ with Protein. The interactions of NAD+ with the enzyme are summarized in Figure 5. The NAD+ binding domain consists of a standard Rossmann nucleotide binding motif of a large twisted β sheet surrounded by α helices. NAD+ is bound in an extended conformation at the C-terminal end of the β sheet. The electron density for the adenine ring and its associated ribose is high in quality, permitting unambiguous identification of the positions of these portions of the cofactor (Figure 5A). Discontinuous electron density was observed for the nicotinamide ring and its associated ribose ring. The conformation and position of the adenine moiety of NADP+ bound to MDH and those of the adenine of the NAD+-bound structure

of *R*-HPCDH are very similar. Although density was rather poor for the nicotinamide in the *R*-HPCDH structure, being able to position the adenine of NAD+ with a high degree of confidence places limited degrees of freedom in the positioning of nicotinamide in the structure. The limited degrees of freedom in combination with the anticipated positioning of nicotinamide with respect to the catalytic triad which is conserved for all SDR enzymes (Ex. MDH) allow a relatively unequivocal assignment of the position of NAD+.

The adenine ring of NAD+ binds in a hydrophobic pocket on the enzyme surface formed by the side chains of Ile90, Val113, Val61, Leu34, Ala88, and Lys109 (Figure 5B). Hydrogen bonds are formed by N1 of adenine and the Asp60 side chain and N6 and the peptide nitrogen of Val61. The Gly9XXXGly13XGly15 sequence corresponding to the classic glycine-rich consensus sequence GlyXXXGlyXGly present in NAD(P)+ binding dehydrogenases can be seen interacting with the adenine ribose of the NAD+ (Figure 5C). Also, the 2′- and 3′-hydroxyl groups of the adenine ribose form hydrogen bonds with an aspartate (Asp33) carboxylate group, which is common for SDR enzymes selectively binding NAD+ and not NADP+ (*32*). The enzymes utilizing NADP+ have a positively charged residue such as arginine at that position to interact with the negatively charged phosphate. The 2′- and 3′-hydroxyl groups of the ribose also interact with Ser12 via hydrogen bonds and indirectly with Ser11
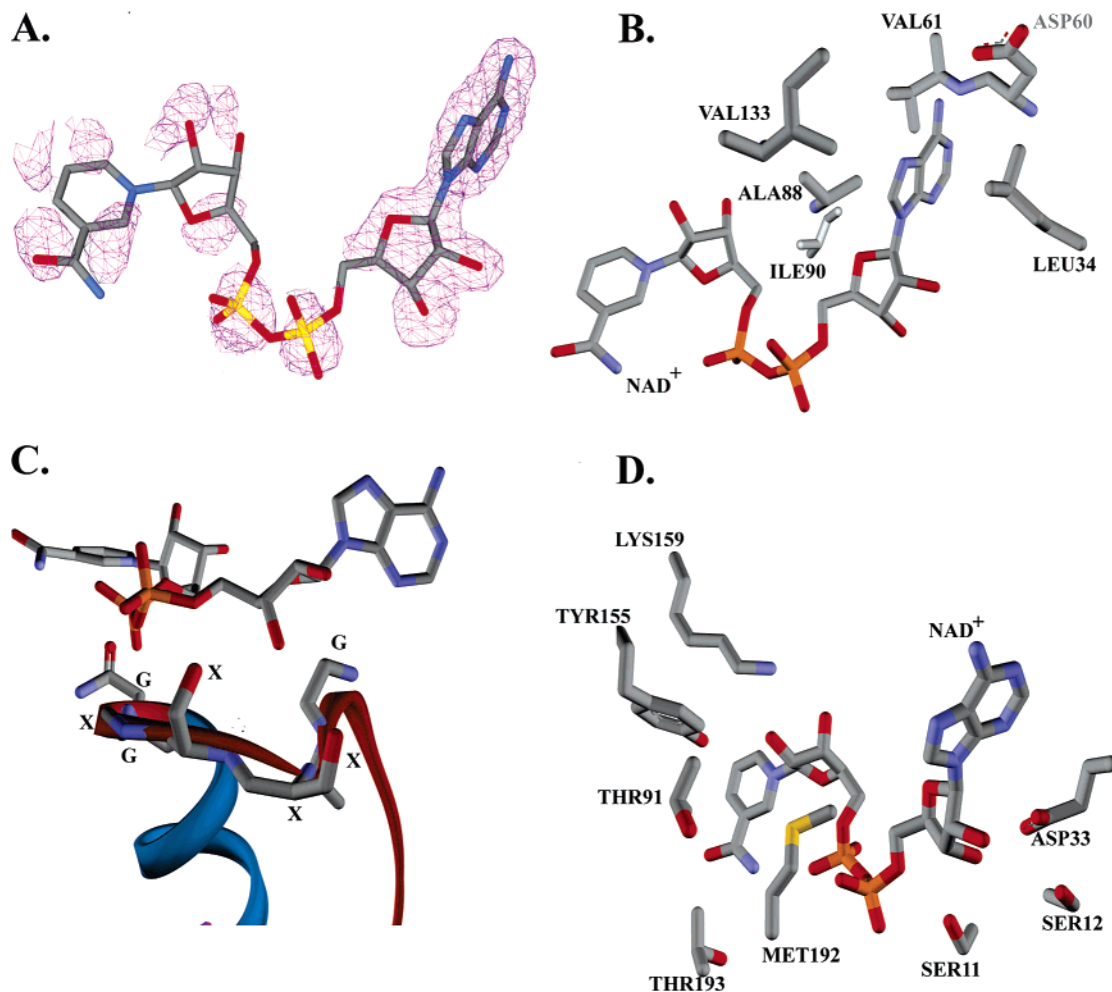
A.

B.

C.

D.

FIGURE 5: (A) Simulated annealing omit electron density map ($2F_o - F_c$) around the NAD$^+$ molecule contoured at 1σ showing unambiguous density around the adenine, the first ribose, and the phosphate and weak density for the nicotinamide ring and the second ribose. (B) Hydrophobic pocket in which the adenine ring of NAD$^+$ resides. The side chains of the amino acids involved in interactions are displayed. (C) Classic GXXXGXG glycine-rich NAD$^+$ binding motif in *R*-HPCDH with NAD$^+$ bound. (D) View of the residues interacting with the nicotinamide ring of NAD$^+$.

through a water molecule. A water molecule at this position is a structural feature of all Rossmann dinucleotide binding domains (*33*). The phosphate groups form hydrogen bonding interactions with side chains of Ser12, Pro191, Met192, Thr190, and Asn14. The 2′- and 3′-hydroxyls of the second ribose (attached to the nicotinamide ring) form a bifurcated hydrogen bond with Lys159. Additional interactions that stabilize the NAD$^+$ in the enzyme include hydrogen bonding of the active site tyrosine with the 3′-hydroxyl of the second ribose and hydrogen bonding between Thr190 and Met192 and the amide group of nicotinamide (Figure 5D).

Substrate Binding Site. Since crystals were grown aerobically in the presence of NAD$^+$ and *S*-HPC, we anticipated that the substrate *S*-HPC would have been largely oxidized to the product 2-KPC during the course of the crystallization. The quality of the electron density maps for the sulfonate and the thioether portion of 2-KPC is excellent, but the ketopropyl moiety of the product is not well resolved (Figure 6A). The product 2-KPC is bound to the enzyme in the aforementioned substrate binding cleft formed by the loop between βF and βG and the loop between βE and βF. This cleft lies directly above the B face of the nicotinamide ring, and the substrate binding site is mainly surrounded by hydrophobic residues. Specific interactions are mainly

between two Arg residues and the product sulfonate. The binding of the product 2-KPC to *R*-HPCDH (Figure 6B) is nearly analogous to the binding of substrate 2-KPC to 2-KPCC (*15*) (Figure 6C). The substrate binding site of *R*-HPCDH is characterized by two methionines (Met192 and Met187) which flank the CoM moiety of the substrate. The sulfonate is bound to two arginine side chains, Arg152 and Arg196, by salt bridge interactions with two methionine residues (Met192 and Met187) that appear to act in shielding the sulfonate charge from the active site. Recent site-directed mutageneses have implicated these arginine residues in sulfonate binding (*14*). These arginines are located on the loops between βE and αE and between βF and αF and approach the substrate and/or product from the sides. Trp195 appears to form a "backstop" that may prevent translation of the substrate and facilitate proper alignment of the substrate with respect to NAD$^+$ for direct hydride transfer. Comparison of the substrate binding site in both of these enzymes suggests a general architecture of flanking methionines, and positively charged amino acids directly binding the sulfonate moiety might be useful in identifying the sulfonate binding site in other CoM-dependent enzymes. To envision how the enzyme binds the substrate, we manually modeled *R*-HPC at the active site by superimposing the
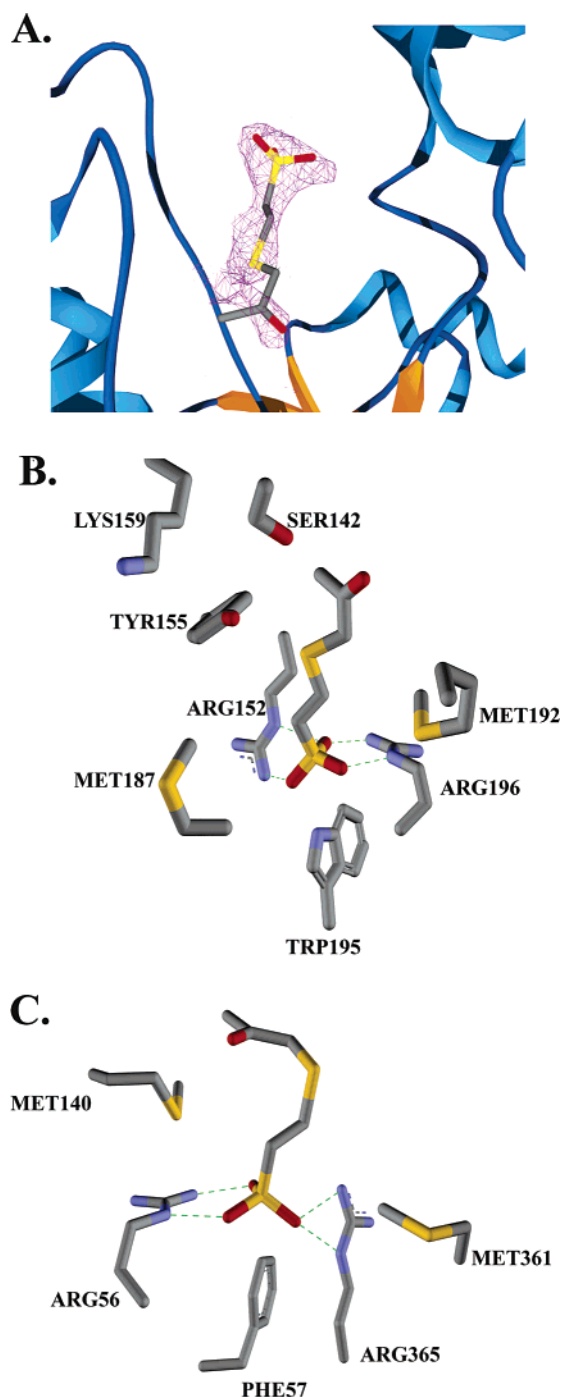
A.

B.

C.

FIGURE 6: (A) Overall view of the product bound in the substrate binding cleft with a $2F_o - F_c$ simulated annealing omit electron density map contoured at 1σ about the product. (B) Product binding at the active site of *R*-HPCDH highlighting the specific interactions with Arg side chains and the adjacent tryptophan residue. The methionines flanking the product are also shown. (C) Substrate binding at the active site of 2-KPCC showing the arginines and the flanking methionines.

FIGURE 7: Wall-eyed stereodrawing of *R*-HPC modeled at the active site of *R*-HPCDH showing active site residues and the nicotinamide ring of the NAD$^+$ molecule.
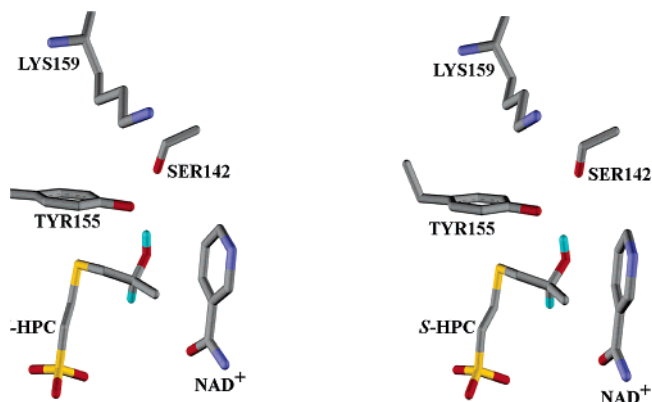
FIGURE 8: Wall-eyed stereodrawing of *S*-HPC bound at the active site of *R*-HPCDH in the same orientation as shown in Figure 7. The nicotinamide part of the NAD$^+$ is shown.

sulfonate moiety and the thioether group of the substrate on those of the product. Orientation of the hydroxyl group of the substrate toward the hydroxyl of Ser142 and Tyr155 resulted in the correct orientation of the hydrogen atom of the substrate toward the NAD$^+$ B face for direct hydride transfer (Figure 7).

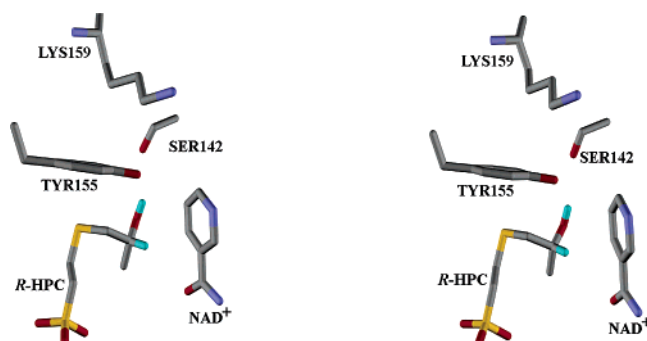   Kinetic analysis shows that *S*-HPC is a very strong competitive inhibitor of *R*-HPCDH with a K_i very similar to the K_m of *R*-HPC (*8*). Although *S*-HPC binds *R*-HPCDH with high affinity, the activity of *R*-HPCDH with *S*-HPC is only 0.1% compared to its activity with *R*-HPC. To visualize the binding mode of *S*-HPC at the active site of *R*-HPCDH, we manually modeled *S*-HPC at the active site by superimposing *S*-HPC on *R*-HPC. Positioning of the hydroxyl group of *S*-HPC exactly over that of *R*-HPC orients the hydrogen atom of *S*-HPC away from NAD$^+$, providing the structural basis for *S*-HPC as a competitive inhibitor (Figure 8).

   Structural Basis for Stereoselectivity. One of the main goals of our structural analysis of the *R*- and *S*-HPCDH enzymes is to reveal the mechanism of chiral discrimination for these enzymes. The specific interactions observed between 2-KPC and *R*-HPCDH in the structure described herein as well as previous biochemical studies suggest that substrate sulfonate binding is the key to orienting the substrate at the active site for hydride abstraction. The structures of both *R*-HPCDH and 2-KPCC illustrate the effectiveness of CoM as a cofactor in this biochemical pathway. If indeed sulfonate binding is the key to correct substrate alignment, then one would expect that sulfonate binding and the specific sulfonate binding sites would be different in *R*-HPCDH and *S*-HPCDH. In fact, the idea that chiral discrimination is conferred through distinct substrate binding sites had been previously proposed on the basis of the results of our biochemical studies and amino acid sequence comparisons (*8*).

   Since a direct crystallographic analysis of *S*-HPCDH has not been possible, the three-dimensional structures of *R*-HPCDH and other SDR enzymes were used to construct a
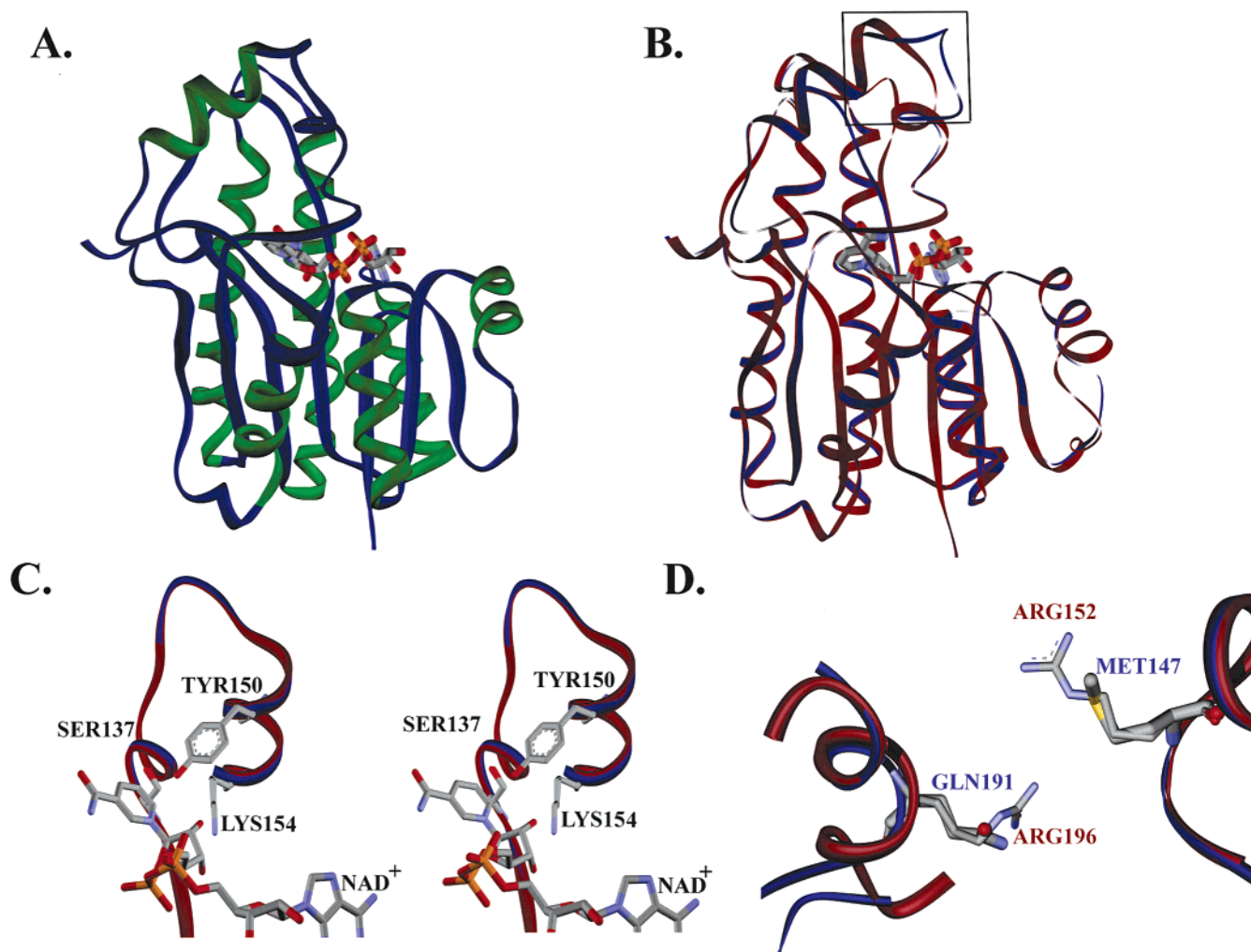
FIGURE 9: (A) Overall tertiary structure of *S*-HPCDH with β strands colored blue and α helices green. NAD⁺ is shown in Corey–Pauling–Koltun (CPK) representation. (B) Superimposition of the structure of *S*-HPCDH (blue) on *R*-HPCDH (dark pink) to show differences in the substrate binding region (boxed area). (C) Close-up view of the active sites of superimposed *R*- and *S*-HPCDH showing a similar orientation of NAD⁺ in both enzymes. The residues of the catalytic triad of the *S*-enantiomer are labeled. (D) Close-up view of *S*-HPCDH superimposed on *R*-HPCDH showing differences in the amino acid residues in the sulfonate binding region. Superimposition was accomplished as described by Kabsch (*32*).

homology model of *S*-HPCDH (Figure 9A). Superimposition of *S*-HPCDH on *R*-HPCDH reveals differences at the substrate binding site that strongly support sulfonate binding as the key to stereoselectivity (Figure 9B). Although residues in the active site are superimposable (Figure 9C), the Arg residues (Arg152 and Arg196) that were observed to be key in binding the sulfonate in *R*-HPCDH have been replaced in *S*-HPCDH with Met147 and Gln191, respectively (Figure 9D). These side chains would not support the binding of the substrate in the same manner that was observed for *R*-HPCDH.

The absence of the sulfonate binding site at that region clearly suggests that the *S*-HPC substrate cannot be bound in a binding mode similar to that of *R*-HPC bound to *R*-HPCDH. Effective hydride abstraction by short chain dehydrogenases is dependent on the correct orientation of the hydride with respect to the nicotinamide and the correct orientation of the substrate hydroxyl group with respect to the Tyr of the catalytic triad. With this in mind, we have utilized the homology model of *S*-HPCDH and the structure of the *S*-HPC substrate to attempt to implicate a sulfonate binding site in this enzyme. To achieve the proper position
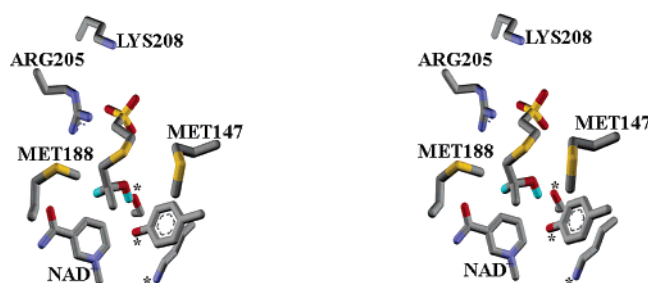

FIGURE 10: Wall-eyed stereopicture of the putative substrate binding site in *S*-HPCDH. The serine-tyrosine-lysine catalytic triad is marked with asterisks. The nicotinamide part of NAD⁺ is shown.

of the substrate hydroxyl and hydrogen, the spatial orientation of the other two groups, namely, the sulfonate and methyl group, must be different in the two enzymes. Since it is hypothesized that differential placement of positively charged residues within the substrate binding region of the enzyme provides the "switch" required for chiral discrimination, the structure of *S*-HPCDH was examined for the presence of a putative sulfonate binding site. Superimposition of *S*-HPC bound to *R*-HPCDH on the NAD⁺-bound structure of

FIGURE 11: Wall-eyed stereopicture of superimposed *R*- and S-HPCDH to show the differential spatial orientation of sulfonate binding sites. The *R*-HPCDH residues and *R*-HPC are colored dark pink, while the *S*-HPCDH residues and *S*-HPC are colored blue.

S-HPCDH followed by rigid body reorientation of the hydroxyl and hydrogen groups with the active site residues and NAD$^+$ puts the sulfonate moiety within hydrogen bonding distance of two positively charged residues (Arg205 and Lys208) (Figure 10). These residues reside on one side of the substrate binding cleft rather than approaching the sulfonate groups from both sides as in the case of *R*-HPCDH. As in the case of both *R*-HPCDH and 2-KPCC, substrate binding is again characterized by two positively charged sulfonate binding groups shielded by two flanking methionine residues (Met147 and Met148). The sulfonate binding sites in *R*- and *S*-HPCDH represent analogous sites involving a different set of amino acid residues at spatially different positions on the respective enzymes. We were able to compare the spatial orientation of this putative sulfonate binding site to that of the sulfonate binding site of *R*-HPCDH to envision the differential placement of positively charged residues that bind the sulfonate moiety of the substrate by superimposing the *S*- and *R*-HPCDH enzymes. Superimposition of *R*- and *S*-HPCDH clearly indicates the differential spatial orientation of the sulfonate binding sites in these two enzymes. From Figure 11, it is clear that although the orientations of active site residues and the NAD$^+$ are exactly same, the sulfonate and the methyl groups are switched to position the hydrogen and hydroxyl groups of the substrate for hydride and proton abstraction, respectively.

The results discussed herein provide a structural basis for chiral discrimination of the *R*- and *S*-HPC substrates by the stereoselective dehydrogenase pair and provide support for our previously proposed model (*14*). Although the overall structure and architecture of both the enzymes are analogous, there are key differences in the substrate binding site. Differential placement of positively charged residues that bind the negatively charged sulfonate group of the substrate in the substrate binding region supports the proper orientation of the hydroxyl and the hydrogen group of the enzyme for proton and hydride abstraction. The sulfonate group is a crucial determinant for orienting the reactive portion of the substrates for chiral discrimination.

REFERENCES

1. Archelas, A., and Furstoss, R. (1997) Synthesis of enantiopure epoxides through biocatalytic approaches, *Annu. Rev. Microbiol. 51*, 491–525.
2. Ensign, S. A. (2001) Microbial metabolism of aliphatic alkenes, *Biochemistry 40*, 5845–5853.
3. Allen, J. R., Clark, D. D., Krum, J. G., and Ensign, S. A. (1999) A role for coenzyme M (2-mercaptoethanesulfonic acid) in a bacterial pathway of aliphatic epoxide carboxylation, *Proc. Natl. Acad. Sci. U.S.A. 96*, 8432–8437.
4. Allen, J. R., and Ensign, S. A. (1996) Carboxylation of epoxides to β-keto acids in cell extracts of *Xanthobacter* strain Py2, *J. Bacteriol. 178*, 1469–1472.
5. Allen, J. R., and Ensign, S. A. (1997) Characterization of three protein components required for functional reconstitution of the epoxide carboxylase multienzyme complex from *Xanthobacter* strain Py2, *J. Bacteriol. 179*, 3110–3115.
6. Allen, J. R., and Ensign, S. A. (1997) Purification to homogeneity and reconstitution of the individual components of the epoxide carboxylase multiprotein enzyme complex from *Xanthobacter* strain Py2, *J. Biol. Chem. 272*, 32121–32128.
7. Allen, J. R., and Ensign, S. A. (1998) Identification and characterization of epoxide carboxylase activity in cell extracts of *Nocardia corallina* B276, *J. Bacteriol. 180*, 2072–2078.
8. Allen, J. R., and Ensign, S. A. (1999) Two short-chain dehydrogenases confer stereoselectivity for enantiomers of epoxypropane in the multiprotein epoxide carboxylating systems of *Xanthobacter* strain Py2 and *Nocardia corallina* B276, *Biochemistry 38*, 247–256.
9. Sauer, K., and Thauer, R. K. (2000) Methyl-coenzyme M formation in methanogenic archaea. Involvement of zinc in coenzyme M activation, *Eur. J. Biochem. 267*, 2498–2504.
10. Jornvall, H., Persson, B., Krook, M., Atrian, S., Gonzalez-Duarte, R., Jeffery, J., and Ghosh, D. (1995) Short-chain dehydrogenases/reductases (SDR), *Biochemistry 34*, 6003–6013.
11. Clark, D. D., and Ensign, S. A. (2002) Characterization of the 2-[(R)-2-hydroxypropylthio]ethanesulfonate dehydrogenase from *Xanthobacter* strain Py2: Product inhibition, pH dependence of kinetic parameters, site-directed mutagenesis, rapid equilibrium inhibition, and chemical modification, *Biochemistry 41*, 2727–2740.
12. Nakajima, K., Hashimoto, T., and Yamada, Y. (1993) Two tropinone reductases with different stereospecificities are short-chain dehydrogenases evolved from a common ancestor, *Proc. Natl. Acad. Sci. U.S.A. 90*, 9591–9595.
13. Nakajima, K., Hashimoto, T., and Yamada, Y. (1994) Opposite stereospecificity of two tropinone reductases is conferred by the substrate-binding sites, *J. Biol. Chem. 269*, 11695–11698.
14. Clark, D. D., Boyd, J. M., and Ensign, S. A. (2004) The stereoselectivity and catalytic properties of *Xanthobacter autotrophicus* 2-[(R)-2-hydroxypropylthio]ethanesulfonate dehydrogenase are controlled by interactions between C-terminal arginine residues and the sulfonate of coenzyme M, *Biochemistry 43*, 6763–6771.
15. Nocek, B., Jang, S. B., Jeong, M. S., Clark, D. D., Ensign, S. A., and Peters, J. W. (2002) Structural basis for CO$_2$ fixation by a novel member of the disulfide oxidoreductase family of enzymes, 2-ketopropyl-coenzyme M oxidoreductase/carboxylase, *Biochemistry 41*, 12907–12913.
16. Nocek, B., Clark, D. D., Ensign, S. A., and Peters, J. W. (2002) Crystallization and preliminary X-ray analysis of an R-2-hydroxypropyl-coenzyme M dehydrogenase, *Acta Crystallogr. D58*, 1470–1473.
17. Garman, E. F., and Mitchell, E. P. (1996) Glycerol concentrations required for cryoprotection of 50 typical protein crystallization solutions, *J. Appl. Crystallogr. 29*, 584–587.

18. Otwinowski, Z., and Minor, W. (1997) in *Methods in Enzymology* (Carter, C. W., Jr., and Sweet, R. M., Eds.) p 20, Academic Press, New York.

19. Terwilliger, T. C., and Berendzen, J. (1999) Automated MAD and MIR structure solution, *Acta Crystallogr. D55* (Part 4), 849−861.

20. Jones, T. A., Zou, J. Y., Cowan, S. W., and Kjeldgaard, M. (1991) Improved methods for building protein models in electron density maps and the location of errors in these models, *Acta Crystallogr. A47* (Part 2), 110−119.

21. Brunger, A. T., Adams, P. D., Clore, G. M., DeLano, W. L., Gros, P., Grosse-Kunstleve, R. W., Jiang, J. S., Kuszewski, J., Nilges, M., Pannu, N. S., Read, R. J., Rice, L. M., Simonson, T., and Warren, G. L. (1998) Crystallography & NMR system: A new software suite for macromolecular structure determination, *Acta Crystallogr. D54* (Part 5), 905−921.

22. Brunger, A. T. (1992) The free *R* value: A novel statistical quantity for assessing the accuracy of crystal structures, *Nature 355*, 472−474.

23. Laskowski, R. A., McArthur, M. W., Moss, D. S., and Thornton, J. M. (1993) PROCHECK: A program to check the stereochemical quality of protein structures, *J. Appl. Crystallogr. 265*, 283−291.

24. Sogabe, S., Yoshizumi, A., Fukami, T. A., Shiratori, Y., Shimizu, S., Takagi, H., Nakamori, S., and Wada, M. (2003) The crystal structure and stereospecificity of levodione reductase from *Corynebacterium aquaticum* M-13, *J. Biol. Chem. 278*, 19387−19395.

25. Lund, O., Nielsen, M., Lundegaard, C., and Worning, P. (2002) X3M: A Computer Program to Extract 3D Models, CASP5 Conference, *Abstract* A102.

26. Gasteiger, E., Gattiker, A., Hoogland, C., Ivanyi, I., Appel, R. D., and Bairoch, A. (2003) ExPASy: The proteomics server for in-depth protein knowledge and analysis, *Nucleic Acids Res. 31*, 3784−3788.

27. Guex, N., and Peitsch, M. C. (1997) SWISS-MODEL and the Swiss-PdbViewer: An environment for comparative protein modeling, *Electrophoresis 18*, 2714−2723.

28. Rossmann, M. G., Liljas, A., Branden, C.-I., and Banaszak, L. J. (1975) in *Evolutionary and structural relationships among dehydrogenases* (Boyer, P. D., Ed.) Academic Press, New York.

29. Tanaka, N. N. T., Nakamura, K. T., and Hara, A. (2001) SDR Structure, Mechanism of Action, and Substrate Recognition, *Curr. Org. Chem.*, 89−111.

30. Horer, S., Stoop, J., Mooibroek, H., Baumann, U., and Sassoon, J. (2001) The crystallographic structure of the mannitol 2-dehydrogenase NADP$^+$ binary complex from *Agaricus bisporus*, *J. Biol. Chem. 276*, 27555−27561.

31. de Jong, R. M., Tiesinga, J. J., Rozeboom, H. J., Kalk, K. H., Tang, L., Janssen, D. B., and Dijkstra, B. W. (2003) Structure and mechanism of a bacterial haloalcohol dehalogenase: A new variation of the short-chain dehydrogenase/reductase fold without an NAD(P)H binding site, *EMBO J. 22*, 4933−4944.

32. Kallberg, Y., Oppermann, U., Jornvall, H., and Persson, B. (2002) Short-chain dehydrogenases/reductases (SDRs), *Eur. J. Biochem. 269*, 4409−4417.

33. Bottoms, C. A., Smith, P. E., and Tanner, J. J. (2002) A structurally conserved water molecule in Rossmann dinucleotide-binding domains, *Protein Sci. 11*, 2125−2137.